

## Deep-level transient spectroscopy of Pd-H complexes in silicon

J.-U. Sachse and J. Weber

*Max-Planck-Institut für Festkörperforschung, Postfach 80 06 65, D-70506 Stuttgart, Germany*

H. Lemke

*TU Berlin, Institut für Werkstoffe der Elektrotechnik, Jebensstraße 1, D-10623 Berlin, Germany*

(Received 24 August 1999)

The interaction of atomic hydrogen with substitutional palladium impurities is studied in *n*- and *p*-type Si by deep-level transient spectroscopy. After wet-chemical etching, we determine seven different electrically active and at least one passive palladium hydrogen complex. The levels belong to Pd complexes with different number of hydrogen atoms. The PdH<sub>1</sub> complex exhibits one level  $E(200)$  at  $E_C - 0.43$  eV. PdH<sub>2</sub> has two levels  $E(60)$  at  $E_C - 0.10$  eV and  $H(280)$  at  $E_V + 0.55$  eV. Four levels are assigned to the PdH<sub>3</sub> complex  $E(160)$  at  $E_C - 0.29$  eV,  $H(140)$  at  $E_V + 0.23$  eV,  $H(55)$  at  $E_V + 0.08$  eV, and  $H(45)$  at  $E_V + 0.07$  eV. An electrically passive complex is associated with a PdH<sub>4</sub> complex. There is great similarity with the correspondent complexes in Pt-doped Si. Annealing above 650 K destroys all hydrogen related complexes and restores the original substitutional Pd concentration.

### I. INTRODUCTION

Transition metals (TM) on substitutional lattice sites in silicon exhibit very similar electronic properties.<sup>1,2</sup> This behavior is commonly attributed to the close structural correspondence of these impurities with the vacancy in silicon.<sup>3</sup> Deep-level transient spectroscopy (DLTS) studies revealed for substitutional palladium and platinum three energy levels a single acceptor level about  $E_C - 0.2$  eV, a single donor level  $E_V + 0.3$  eV, and a double donor level at approximately  $E_V + (0.1 - 0.15)$  eV.<sup>4,5</sup>

Recently, the effect of hydrogen on the electrical properties of transition metals in silicon, especially the formation of electrically active complexes, has stimulated many studies.<sup>6-15</sup> The interaction of hydrogen and platinum in silicon has been the subject of several reports.<sup>16-19</sup> In particular, a PtH<sub>2</sub> complex with two acceptor levels in the band gap was identified by electron paramagnetic resonance (EPR) and vibrational spectroscopy.<sup>18</sup> DLTS measurements combined with depth-profile and annealing studies showed that platinum forms several hydrogen related complexes after hydrogenation by wet-chemical etching.<sup>19,20</sup> The complexes differ in the number of hydrogen atoms, most of them are electrically active, but at least one complex PtH<sub>4</sub> was proposed to be electrically neutral. This behavior is in contrast to an earlier study by Pearton and Haller.<sup>21</sup> After heat treatment in a hydrogen plasma at 300 °C, these authors reported a reduction of the concentration of the Pt acceptor level, which they explained with the passivation by hydrogen. They observe, however, no indication for electrically active PtH defects. In the same study a complete passivation was reported for both the palladium donor and acceptor level by hydrogen plasma treatment.<sup>21</sup> To our knowledge, this is the only report about the effect of hydrogen on palladium in silicon. Since the isolated substitutional defects of palladium and platinum show a very close electronic relationship, one can expect similarities in the interaction of both metals with hydrogen.

In this paper, we present evidence for hydrogen related

electrically active and passive palladium complexes in silicon and show their evolution after thermal treatments. Based on a model of hydrogen diffusion and capture by traps, we identify from the concentration depth profiles of the PdH complexes the number of H atoms involved in the complexes. Finally, we compare the results with platinum hydrogen complexes in silicon. A preliminary account of our work was already given in Ref. 22.

### II. EXPERIMENT

We used phosphorus- or boron-doped float zone or Czochralski silicon with doping concentration in the range of  $1 \times 10^{14}$  to  $1 \times 10^{16}$  cm<sup>-3</sup>. Palladium was incorporated either by introducing the metal directly into the silicon melt during crystal growth of float-zone silicon<sup>23</sup> or by diffusion at temperatures between 900 °C and 1000 °C from thin metal films, which were evaporated onto one side of a polished Si wafer. The total concentration of electrically active Pd atoms reached  $1 \times 10^{13}$  to  $5 \times 10^{14}$  cm<sup>-3</sup>. Hydrogenation of the samples was performed by wet-chemical etching in a 1 : 2 : 1 mixture of HF, HNO<sub>3</sub>, and CH<sub>3</sub>COOH before contact preparation. The Schottky contacts were prepared by aluminum (*p*-type samples) or gold (*n*-type samples) evaporation at room temperature. The ohmic contact was formed by rubbing an eutectic InGa alloy onto the back side of the samples. In addition, hydrogenation during wet-chemical etching was avoided by cleaving the samples and evaporating the contacts directly onto the sample surfaces without any additional surface treatment. The cleaved samples did not show any hydrogen contamination.

Annealing experiments up to 450 K were performed with Schottky contacts on the samples. At higher temperatures the quality of the Schottky diodes deteriorated resulting in a drastic increase of the leakage current. Therefore, these samples were first etched, followed by the annealing treatment in argon ambient. Finally, the Schottky contacts were

evaporated without any additional etching before the metalization.

The samples were characterized electrically using deep-level transient spectroscopy and minority-carrier transient spectroscopy (MCTS). DLTS was performed by measuring the capacitance transients directly with a transient recorder or by integration with a lock-in amplifier. We will label DLTS levels of unknown origin by  $A(T)$ .  $A=E$  indicates electron emission and  $A=H$  stands for hole emission;  $T$  is the temperature at maximum peak height (emission rate equals  $42 \text{ s}^{-1}$ ). The shallow dopant concentration profiles are determined by capacitance-voltage (CV) profiling (1 MHz). The distribution of the deep levels was measured by DDLTS (double pulse DLTS) concentration profiling.<sup>24</sup> The profiles are calculated taking into account nonuniform shallow dopant profiles due to hydrogen passivation of the dopants. The error in the deep-level concentration is in the order of 5% of the values given in the figures. The capture cross sections of majority carriers were extracted from the electron- or hole-capture rates that were measured by variation of the filling pulse length.<sup>25</sup>

The behavior of deep levels in the other half of the band gap, which cannot be probed by DLTS on Schottky diodes, was studied by MCTS measurements. In this technique the electrical filling pulse of DLTS is replaced by an optical pulse of above band-gap light. The generated minority carriers are captured by deep levels. Details of the technique were described elsewhere.<sup>26,27</sup> We used a GaAs double heterostructure diode as light source (wavelength 850 nm) and illuminated the samples through the front side Schottky contacts. The minority-carrier transients were integrated by a boxcar averager. The low-temperature limit of the cryostat for the MCTS scans was 90 K.

### III. RESULTS

#### A. Palladium related deep levels in $p$ -type silicon

##### 1. Basic features of PdH complexes

A typical DLTS spectrum of a palladium-doped  $p$ -type sample directly after wet-chemical etching is shown in Fig. 1, curve (a). We observe two dominant peaks with identical depth profiles at 70 K and 165 K. The activation energy and the hole-capture cross section of the peak at 165 K agrees with the values reported for the single donor level of substitutional palladium  $\text{Pd}^{0/+}$ .<sup>21,28–32</sup> Previously, we could demonstrate that the peak at 70 K can be assigned to the double donor level of substitutional palladium in silicon  $\text{Pd}^{+/++}$ .<sup>5</sup> The electrical data of both levels are given in Table I. The activation energy of the Pd double donor level is reduced by the electrical field in the space-charge region, and its capture cross section is thermally activated with an activation energy of 30 meV. The single donor level shows no electric-field dependence of the activation energy and no thermally activated capture cross section.<sup>5</sup>

In addition, another small peak at 280 K labeled H(280) is detected in the spectrum of Fig. 1(a). This signal increases with annealing at 370 K for 30 min [Fig. 1(b)] while the substitutional Pd peaks decrease by the same amount. An increase in the annealing temperature results in a further enhancement of H(280) as shown in Fig. 1(c) for a 30 min

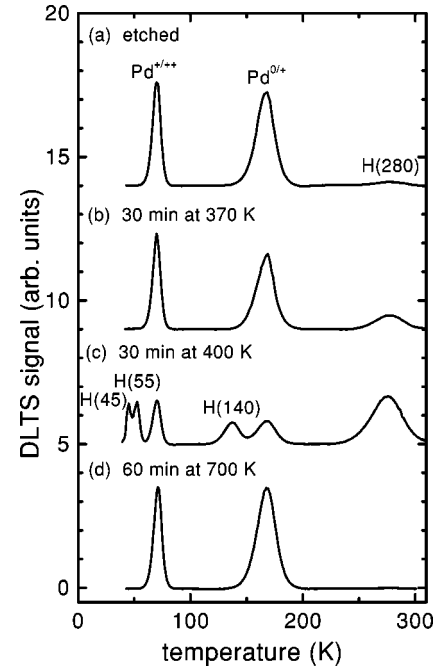


FIG. 1. DLTS spectra of Pd-doped  $p$ -type Si ( $e_n = 42 \text{ s}^{-1}$ ,  $V_r = -2 \text{ V}$ ,  $t_f = 3 \text{ ms}$ ). (a) After etching, (b) after etching and subsequent zero-bias annealing at 370 K for 30 min, (c) after etching and subsequent annealing at 400 K for 30 min, (d) after etching and subsequent annealing at 700 K for 30 min.

treatment at 400 K. Both Pd donor levels are reduced significantly, and three new peaks appear in the spectrum labeled H(45), H(55), and H(140). H(45) and H(55) have always the same intensity; however, the capture cross section of H(45) is remarkably small (see Table I), long filling pulses ( $t_f \geq 3 \text{ ms}$ ) are needed to fill this center completely. Furthermore, we observe an increase of the emission rate of H(45) with increasing electric field. The other newly formed cen-

TABLE I. Energy levels  $E_A$  determined from Arrhenius plots of emission rates, capture cross sections  $\sigma_{n,p}$  determined by variation of the filling pulse length, level character, and assignment of the deep levels based on the analysis of the depth profiles. The capture cross sections of levels  $E(60)$ , H(45), and the Pd double donor are thermally activated and can be described by Eq. (1). The listed values correspond to the prefactors  $\sigma_\infty$ . The value for H(45) could not be measured. The level character is determined from the electrical-field dependence of the level positions and in analogy to the PdH complexes.

Level	$E_A$ (eV)	$\sigma_{n,p}$ ( $\text{cm}^2$ )	Character	Assignment
$E(60)$	$E_C - 0.18$	$3 \times 10^{-15}$	— / —	$\text{PdH}_2$
Pd acceptor	$E_C - 0.23$	$3 \times 10^{-15}$	— / 0	$\text{Pd}_5$
$E(160)$	$E_C - 0.29$	$2 \times 10^{-16}$	?	$\text{PdH}_3$
$E(200)$	$E_C - 0.43$	$7 \times 10^{-16}$	— / 0	$\text{PdH}_1$
H(280)	$E_V + 0.55$	$2 \times 10^{-17}$	— / 0	$\text{PdH}_2$
Pd donor	$E_V + 0.31$	$6 \times 10^{16}$	0 / +	$\text{Pd}_5$
H(140)	$E_V + 0.55$	$2 \times 10^{-17}$	— / 0	$\text{PdH}_3$
Pd double donor	$E_V + 0.14$	$5 \times 10^{-15}$	+ / ++	$\text{Pd}_5$
H(55)	$E_V + 0.08$	?	?	$\text{PdH}_3$
H(45)	$E_V + 0.07$	$1 \times 10^{-18}$	+ / ++	$\text{PdH}_3$

ters do not show any field dependence of their activation energies or a temperature dependence of the capture cross section.

Annealing at temperatures between 450 and 550 K results in a decrease of all observed peaks without the appearance of new signals. H(45), H(55), and H(140) anneal out completely during a 1 h heat treatment at 550 K. H(280) is more stable but disappears after 1 h at 700 K as shown in Fig. 1(d). At temperatures  $T \geq 550$  K both Pd donor levels start to recover, and after 1 h annealing at 700 K their intensities reach the initial values detected directly after etching [compare curves (a) and (d) in Fig. 1].

Levels H(280), H(140), H(55), and H(45) are formed only in Pd-doped samples after wet-chemical etching and subsequent annealing. This behavior strongly suggests that the new levels are palladium hydrogen related defects. In contrast, the cleaved samples that are free from hydrogen show only the two Pd donor levels, an additional anneal of the samples up to 470 K did not change the DLTS spectra.<sup>5</sup>

## 2. Depth profiles of PdH centers and the effect of reverse bias annealing

Charged hydrogen drifts during reverse bias annealing (RBA) from the surface into the bulk of the sample. A typical example is given in Fig. 2(a). The solid line represents the profile of the net boron acceptor concentration directly after etching. The passivation of boron at depths  $\leq 5 \mu\text{m}$  is caused by the introduction of hydrogen during the etching and the formation of electrically inactive boron hydrogen pairs.<sup>33</sup> An annealing step at 370 K using a reverse bias of  $-8$  V leads to the dissociation of BH pairs resulting in the reactivation of boron close to the sample surface. The released positively charged hydrogen drifts to the end of the space-charge region and forms there new BH pairs causing the dip in the net boron concentration at a depth of  $12 \mu\text{m}$  [dashed line in Fig. 2(a)].

The depth profiles of the deep levels directly after etching are given in Fig. 2(b). The Pd single and double donor profiles are uniform and coincide. This behavior is found in all samples that were doped during the float-zone process. Level H(280) is only detectable close to the sample surface where hydrogen has been incorporated. A subsequent RBA step affects the depth profiles dramatically [see Fig. 2(c)]. Level H(280) forms deeper in the bulk with a maximum concentration at a depth of  $12 \mu\text{m}$ . This depth coincides well with the end of the space-charge region, where most of the hydrogen can be found after the RBA [compare Fig. 2(a)]. The changes in the profiles with RBA show that the formation of H(280) is controlled by the movement of  $\text{H}^+$ . This behavior supports again the identification of this level as due to a hydrogen complex. The increase of H(280) is accompanied by an equal reduction in the substitutional palladium concentration. This mirrorlike behavior proves that H(280) belongs to a palladium hydrogen complex containing only one Pd atom.

The levels formed at higher temperatures [H(45), H(55), and H(140)] behave similarly under RBA. This is shown in Fig. 2(d) for a RBA step at 400 K using the same reverse bias as in Fig. 2(c). The depth profiles of all three levels have their concentration maxima at the end of the depletion region where hydrogen is concentrated. At the same time the dip in

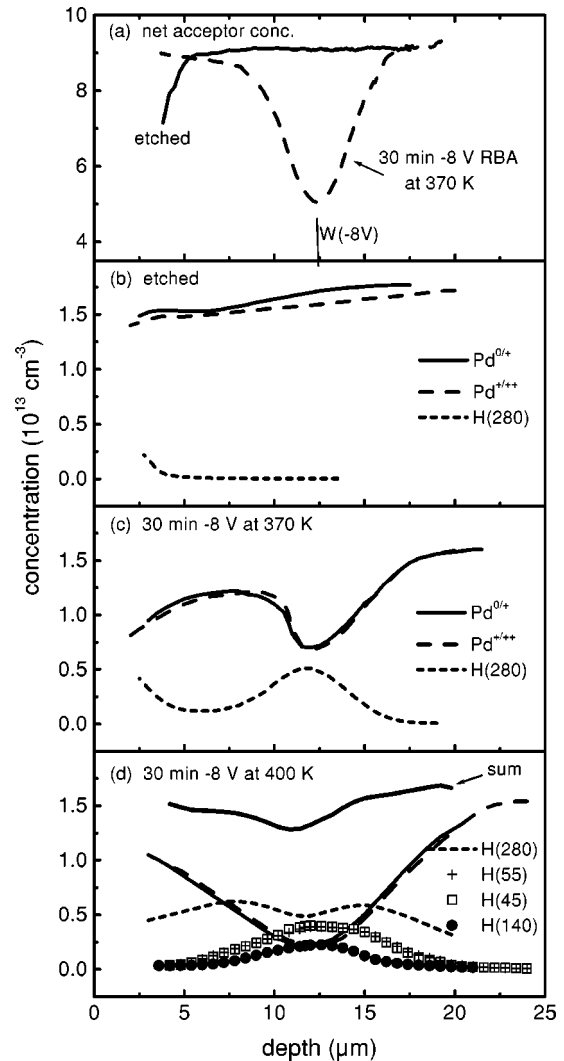


FIG. 2. Depth profiles of defects in Pd-doped  $p$ -type Si. (a) Boron profile directly after wet-chemical etching and after reverse bias anneal (RBA) at 370 K. ( $V_{\text{bias}} = -8$  V,  $t = 30$  min) (b) Pd donor  $\text{Pd}^{0/+}$ , double donor  $\text{Pd}^{+/++}$ , and H(280) profiles after wet-chemical etching, (c) same as (b) plus additional RBA (30 min at 370 K,  $V_{\text{bias}} = -8$  V), (d) same as (b) plus additional RBA (30 min at 400 K,  $V_{\text{bias}} = -8$  V).

the concentration of the Pd donors has increased drastically. This leads us to the conclusion that H(45), H(55), and H(140) are also palladium hydrogen related. The profiles of H(45) and H(55) coincide, and studies at different temperatures between 400 and 550 K confirm this behavior, suggesting that both levels belong to the same PdH complex. Reverse bias annealing at higher temperatures up to 550 K leads to the decrease of all three PdH related levels. However, H(140) seems to be slightly more stable since after a 1 h heat treatment at 500 K its concentration exceeds the corresponding values of H(45) and H(55). The intensity changes of H(140) relative to H(45) and H(55) are related to the reverse bias annealing conditions. After RBA we usually cool down the samples with applied reverse bias. If we cool down without reverse bias, we always get the same intensity of the three levels. Annealing the samples without applied reverse bias leads in all cases to very similar profiles for H(140), H(55), and H(45). This behavior is evidence for a

structural metastability of the same PdH complex. Cooling down the sample with applied reverse bias favors the formation of the configuration with the  $H(45)/H(55)$  level. A detailed study of the metastability is necessary to clarify the nature of the two configurations.

In contrast to  $H(45)$ ,  $H(55)$ , and  $H(140)$ , which are concentrated in the hydrogen-rich region, level  $H(280)$  can be detected in a much wider range after RBA at 400 K [see dotted line in Fig. 2(d)]. Level  $H(280)$  shows however a dip in the concentration where the other levels exhibit a maximum. This indicates that part of the  $H(280)$  centers transform into  $H(45)$ ,  $H(55)$ , and  $H(140)$ , respectively.

Based on the characteristic depth profiles and thermal stabilities, we assign the four hydrogen-related levels  $H(45)$ ,  $H(55)$ ,  $H(140)$ , and  $H(280)$  to three different electrically active PdH complexes. The total concentration of palladium resulting from the sum of the levels  $\text{Pd}^{0+}$ ,  $H(55)$ ,  $H(140)$ , and  $H(280)$  is also shown in Fig. 2(d) (labeled sum). The concentration of levels  $H(45)$  and  $\text{Pd}^{+/++}$  have not been considered for the summation since they belong to the same defect as  $H(55)$  and  $\text{Pd}^{0+}$ , respectively. We find that the total concentration of all electrically active Pd centers equals the Pd concentration in the etched sample [compare Fig. 2(b)], this indicates that not only  $H(280)$  but all the hydrogen complexes contain only one Pd atom. However, a dip in the total Pd concentration is detected in the region where hydrogen has been piled up. Heat treatments at higher temperatures increase the dip further. This indicates that a portion of palladium is not detected by DLTS, i.e., some palladium centers are either electrically inactive or have at least no deep levels in the lower half of the band gap. We will show later on that this inactive Pd center belongs to another PdH complex, which is electrically passive. The passive complex grows at the expense of all other hydrogen complexes and reaches the maximum concentration at annealing temperatures around 500 to 550 K. The thermal stability of the passive complex is very similar to the  $H(280)$  level. Further increase in temperature destroys the passive complex and reactivates the isolated Pd levels, without forming the  $H(280)$  level again.

## B. Palladium-related centers in $n$ -type silicon

### 1. DLTS spectra of palladium doped $n$ -type silicon

In  $p$ -type Si we find very similar DLTS spectra for cleaved and etched Pd-doped samples. Only after a heat treatment, significant differences occur due to the formation and increase of hydrogen-related centers in the etched samples. In  $n$ -type Si, however, we observe already after etching a dramatic difference in the DLTS spectrum as shown in Fig. 3. Curve (a) represents the spectrum of a cleaved Pd-doped  $n$ -type sample. Only one peak at 115 K is detected. The activation energy and the electron-capture cross section of this DLTS level (shown in Table I) agree with the values reported on the acceptor level of substitutional palladium  $\text{Pd}^{-/0}$ .<sup>21,28–32,34,35</sup> After etching, the Pd acceptor concentration decreases significantly while three other peaks appear in the spectrum labeled  $E(60)$ ,  $E(160)$ , and  $E(200)$ . The corresponding values for the activation energies and capture cross sections are presented in Table I. It should be noted that the electron-capture cross section of level

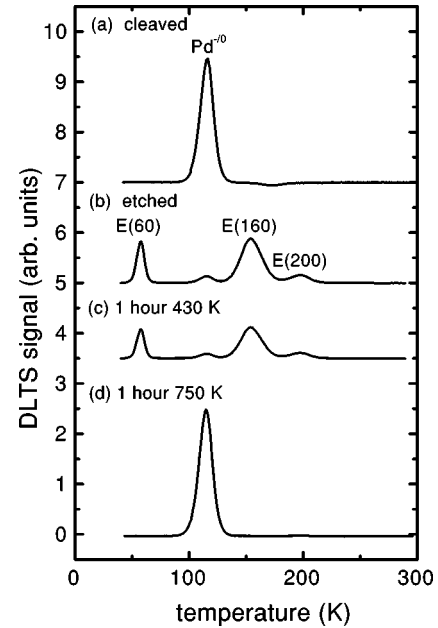


FIG. 3. DLTS spectra of Pd-doped  $n$ -type Si. (a) Cleaved sample, (b) after wet-chemical etching, (c) same as (b) plus subsequent zero-bias annealing at 400 K for 1 h, (d) same as (b) plus subsequent annealing at 650 K for 1 h.

$E(60)$  is very small but depends strongly on the temperature (Fig. 4). The dependence follows the relation

$$\sigma_n = \sigma_{n\infty} \exp[-E_{\text{on}}/kT], \quad (1)$$

with an activation energy  $E_{\text{on}}$  of about 40 meV. Taking this energy into account leads to a significant reduction of the activation enthalpy (see Table I). Furthermore, we find a reduction of the activation energy of this level with increasing electric field. Usually, this property associates the level in  $n$ -type Si to a single donor state, which shows an attractive Coulomb interaction with the emitted carriers. However, field-induced reduction of the activation energy has also been observed for repulsive centers such as the double donor levels of platinum<sup>4</sup> and palladium<sup>5</sup> in  $p$ -type samples. For these levels the field dependence was always accompanied by a thermally activated capture cross section.<sup>5</sup> Since the

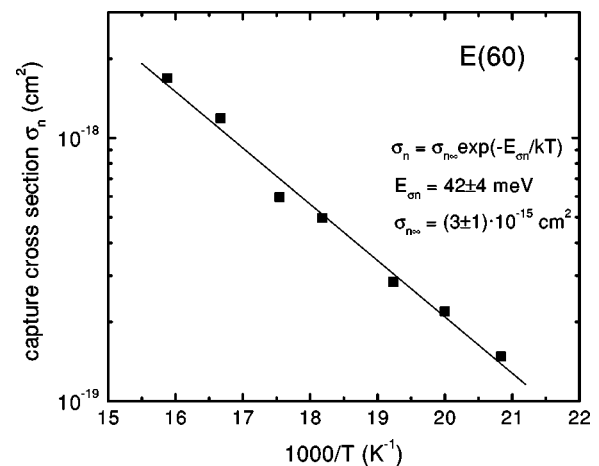


FIG. 4. Temperature dependence of the capture cross section of level  $E(60)$ .

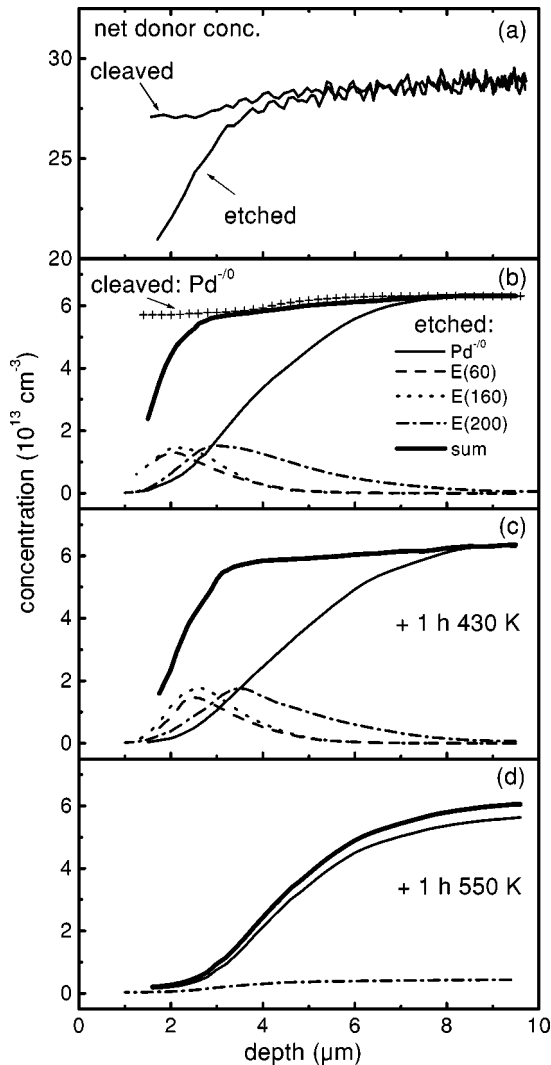


FIG. 5. Depth profiles of defects in Pd-doped *n*-type Si. (a) Phosphorus profile in the cleaved sample and directly after wet-chemical etching, (b) depth profiles of the platinum-related defects  $\text{Pd}^{-/0}$ ,  $E(60)$ ,  $E(160)$ , and  $E(200)$  after etching. The sum of the concentrations of these defects is also shown. (c) Same as (b) plus additional annealing at 430 K for 1 h. (d) Same as (b) plus additional annealing at 550 K for 1 h.

capture cross section of  $E(60)$  is also thermally activated, we assign this level to a repulsive center, i.e., a double acceptor.

Annealing the samples at temperatures up to 400 K does not alter the spectrum. An increase of the annealing temperature to 430 K results, however, in the decrease of all peaks [Fig. 3(c)] while no other new signal appears in the spectrum. The levels  $E(60)$  and  $E(160)$  anneal out completely between 500 and 550 K while  $E(200)$  disappears at 650 K. At temperatures above 550 K, the Pd acceptor recovers, and after a 1 h heat treatment at 750 K the acceptor has regained its original concentration.

## 2. Depth profiles and annealing behavior of PdH complexes

The levels  $E(60)$ ,  $E(160)$ , and  $E(200)$  are formed directly after wet-chemical etching, which indicates that they are all hydrogen related. This assignment is supported by the evaluation of the concentration depth profiles given in Fig. 5.

Figure 5(a) shows the depth profiles of the net phosphorus donor concentration before (cleaved sample) and directly after etching. For the cleaved sample, we observe a flat profile, while a significant reduction of the net active phosphorus concentration is observed after etching in the region close to the surface (at depths  $\leq 4 \mu\text{m}$ ). The reduction is caused by the formation of passive phosphorus hydrogen pairs<sup>36,37</sup>. The profile of the etched sample after annealing at 430 K for 1 h is identical to the profile of the cleaved sample.

The corresponding depth profiles of the palladium-related deep levels are compared in Fig. 5(b). The cleaved sample has a uniform palladium acceptor profile [crosses in Fig. 5(b)]. After etching the Pd acceptor concentration decreases towards the surface, and the three additional palladium-related levels appear:  $E(60)$ ,  $E(160)$ , and  $E(200)$ . All three levels have their maximum concentration within the depth where hydrogen has diffused in ( $2\text{--}3 \mu\text{m}$ ) and decrease towards the bulk and the surface. The profiles of  $E(60)$  and  $E(160)$  are very similar after etching, while the profile of  $E(200)$  is always shifted deeper into the bulk. Since level  $E(60)$  decreases slightly faster during annealing at temperatures above 500 K, we assign the three hydrogen-induced levels to three different PdH complexes. The sum of the concentrations of all Pd-related levels [ $\text{Pd}^{-/0}$ ,  $E(60)$ ,  $E(160)$ , and  $E(200)$ ] after etching is also shown in Fig. 5(b). The total concentration of electrically active palladium is uniform at depths  $\geq 3 \mu\text{m}$  and equals the value in the cleaved sample. The behavior indicates again that only one Pd atom is involved in each PdH complex. Close to the sample surface we observe a decrease in the sum profile, which we correlate with the formation of an electrically passive PdH complex.

In *p*-type Si we used the dissociation of the acceptor hydrogen pairs and the drift of the released positively charged hydrogen in an applied electric field to localize the hydrogen and correlate it with the distribution of the deep levels (see Fig. 2). This method cannot be applied in moderately doped *n*-type material since an annealing under reverse bias results only in the dissociation of neutral phosphorus hydrogen pairs close to the sample surface and the reactivation of phosphorus donors, but no inwards drift of a hydrogen species can be detected.<sup>19,36,37</sup> Annealing studies on Pd-doped *n*-type samples at temperatures up to 400 K confirm these results. Furthermore, we find that the profiles of all Pd-related levels remain unchanged compared to Fig. 5(b).

An increase of the annealing temperature results, however, in a small inwards shift of all trap profiles as shown in Fig. 5(c) for a 1 h heat treatment at 430 K. The concentrations of the PdH-related levels  $E(60)$ ,  $E(160)$ , and  $E(200)$  are slightly increased at depths  $\geq 3.5 \mu\text{m}$  while the passivation of the Pd acceptor reaches deeper into the bulk. At depths  $\leq 2.5 \mu\text{m}$  the concentrations of all electrically active deep levels are reduced. We explain this shift by the indiffusion of hydrogen from the surface region towards the bulk. The incoming hydrogen reacts with substitutional Pd and the already formed PdH complexes. Close to the surface the passive PdH complex expands deeper into the bulk at the cost of all electrically active Pd-related centers. At greater depths hydrogen forms more electrically active complexes with substitutional Pd, this explains the increase of the concentration of  $E(60)$ ,  $E(160)$ , and  $E(200)$ . The source of the additional

hydrogen is not yet clear, but the hydrogen release from the dissociation of phosphorus hydrogen pairs should be ruled out since these pairs are already destroyed during annealing at much lower temperatures.

Heat treatments at temperatures above 500 K result in a further expansion of the passive palladium hydrogen complex into the bulk [Fig. 5(d)]. At the same time the concentration maxima of the electrically active PdH centers shift further inwards accompanied by a decrease in concentration. After a 1 h heat treatment at 550 K, both  $E(60)$  and  $E(160)$  are completely annealed out while level  $E(200)$  is slightly more stable. Above 550 K we observe a gradual reactivation of the Pd acceptor concentration and a decrease of the passive complex. The resulting Pd profile after 1 h annealing at 700 K is flat, and the concentration reaches the value in the cleaved sample.

### 3. MCTS measurements on Pd-doped $n$ -type silicon

The DLTS technique enables us to probe defect levels in the lower half of the band gap in  $p$ -type silicon and in the upper half of the band gap in  $n$ -type silicon, respectively. In order to correlate different PdH levels, it is necessary to determine in the same sample the properties of all levels in the band gap. This can be achieved by the injection of minority carriers as performed in MCTS measurements. Minority carriers generated by above band-gap light in the neutral region close to the depletion region of a reverse biased Schottky diode diffuse into the space-charge region of the Schottky contact where they are available for capture by deep levels.

Since the samples were illuminated through the Schottky contact the effect of majority carriers cannot be neglected. Majority carriers that are generated in the neutral region are rejected from the depletion layer by the electric field. However, majority carriers that are created within the space-charge region may be captured by traps. This results in a normal majority-carrier DLTS contribution to the MCTS spectrum and has to be included in the evaluation of the spectra.

The quality of the MCTS spectrum depends strongly on the surface conditions. In particular, MCTS measurements on Pd-doped  $p$ -type Si samples were not successful due to a large background signal. However, we succeeded to detect minority-carrier traps in Pd-doped  $n$ -type samples as shown in Fig. 6. The spectra are measured after wet-chemical etching using two different reverse voltages. We find three different MCTS peaks at 140 K, 170 K, and 280 K. Their activation energies agree with the values determined by DLTS for H(140), Pd<sup>0/+</sup>, and H(280) (see Table I). It should be noted that level H(140) appears in  $n$ -type Si already after etching while in  $p$ -type material an additional heat treatment is necessary to form the center.

Due to restrictions of the MCTS apparatus, we were limited to temperatures above 90 K. Therefore, we could not probe the temperature range where the Pd double donor and the hydrogen-related levels H(45) and H(55) appear in  $p$ -type Si. Furthermore, we observe a dip at about 115 K in both spectra of Fig. 6. We assume that this is caused by the capture and subsequent emission of majority carriers from the Pd acceptor level. Thus, this peak corresponds to a majority-carrier DLTS peak superimposed on the MCTS background signal.

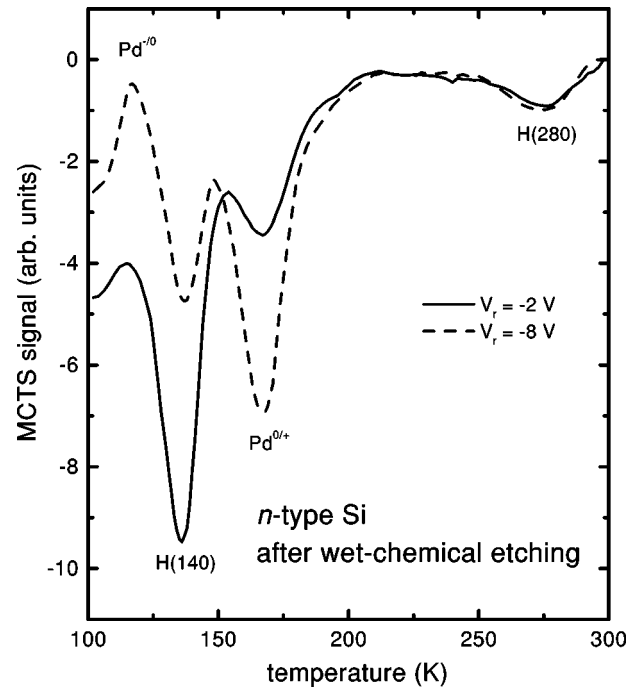


FIG. 6. MCTS spectra at two different reverse bias voltages ( $V_{\text{bias}} = -2$  V and  $-8$  V) for Pd-doped  $n$ -type Si directly after wet-chemical etching.

The determination of quantitative depth profiles from the variation of the electrical filling pulse height is not possible with our method of MCTS. However, qualitative information about the depth distribution of the defects is possible by MCTS measurements under different reverse biases (see Fig. 6). We note that the MCTS peak of level H(140) is larger closer to the surface ( $V_r = -4$  V) and smaller in the bulk ( $V_r = -8$  V). This behavior is expected for a hydrogen-related level and confirms the DLTS depth profiling results on annealed Pd-doped  $p$ -type samples. The signal of the Pd donor shows an increase towards the bulk. The intensity of H(280) is much lower than H(140), which indicates that the H(280) can also capture electrons. A capture of an electron in a trap already filled with a hole leads to the recombination of both carriers resulting in the loss of the hole. Thus hole emission from this trap would be reduced if electrons are available for capture. Figure 6 also shows the Pd acceptor Pd<sup>0/+</sup> as a majority-carrier trap. The other hydrogen-related levels  $E(160)$  and  $E(200)$  known from  $n$ -type Si are not detected. In the case of  $E(160)$ , it is possible that this signal overlaps strongly with H(140) and Pd<sup>0/+</sup> and is therefore not resolvable. The concentration of level  $E(200)$  is usually very low directly after etching [see Fig. 3(b)] and a detection is not possible.

## IV. DISCUSSION

### A. The formation of hydrogen complexes

The depth profiles of hydrogen complexes created by wet-chemical etching in irradiated Si were recently interpreted by Feklisova and Yarykin.<sup>38</sup> The complex formation is understood as a subsequent addition of hydrogen atoms to the defects. The following set of equations describes the step by step hydrogenation:

$$\frac{d[A_0]}{dt} = -4\pi D r_o [A_0][H], \quad (2)$$

$$\frac{d[A_i]}{dt} = 4\pi D (r_{i-1}[A_{i-1}] - r_i[A_i])[H],$$

$$i = 1, 2, 3, \dots,$$

where  $A_i$  is the complex with  $i$  hydrogen atoms,  $r_i$  is the capture radius of hydrogen to the  $A_i$  complex, and  $[H]$  and  $D$  the concentration and the diffusivity of atomic hydrogen, respectively.

The differential equations for the hydrogen complexes can be solved analytically in the limit of large depth, provided that all complexes are thermally stable, i.e., a hydrogen atom once captured remains attached to the complex and the concentration of the different hydrogen defects decreases with the number of hydrogen atoms ( $[A_i] \gg [A_{i+1}]$ ). The approximations lead to a simple exponential decay of the defect concentration,

$$[A_i] \sim \exp\left(-\frac{x}{L_i}\right), \quad (3)$$

with a characteristic length  $L_i$  that is derived to be inversely proportional to the number  $i$  of hydrogen atoms

$$L_i \approx 1/i. \quad (4)$$

The simple relation was used to analyze the depth profiles of PtH complexes in Si. Although, the model was originally developed for profiles that are found directly after wet-chemical etching, we could apply the formalism even in the case of thermally annealed samples.<sup>20</sup> A numerical integration of Eq. (3) is possible for different experimental conditions, e.g., after wet-chemical etching, after annealing, etc. In all cases, we find in the limit of larger depth the simple exponential behavior. A detailed investigation of the numerical fitting of the total depth profiles will be published elsewhere.

## B. Analysis of the PdH depth profiles

### 1. *n*-type samples

We detect by DLTS in Pd-doped Si after wet-chemical etching seven other hydrogen-induced levels. The electrical data of all levels are summarized in Table I. The assignment of different levels to the same defect based on the thermal stability is not possible in our samples. The annealing behavior is not a first-order process, and the temperature where levels disappear is determined by capture of hydrogen to different complexes. A direct connection of different levels to the same defect is, however, possible from a comparison of the depth profiles. Ideally, levels of the same defect should exhibit the identical profile. For the PtH complexes such a simple behavior was detected.<sup>20</sup>

A comparison of the depth profiles in *n*- and *p*-type samples is only reasonable if the influence of the shallow dopant as trapping centers is neglected. The formation of hydrogen complexes is quite different after etching or after low-temperature annealing. Therefore, we use for comparison only those profiles that were determined in samples an-

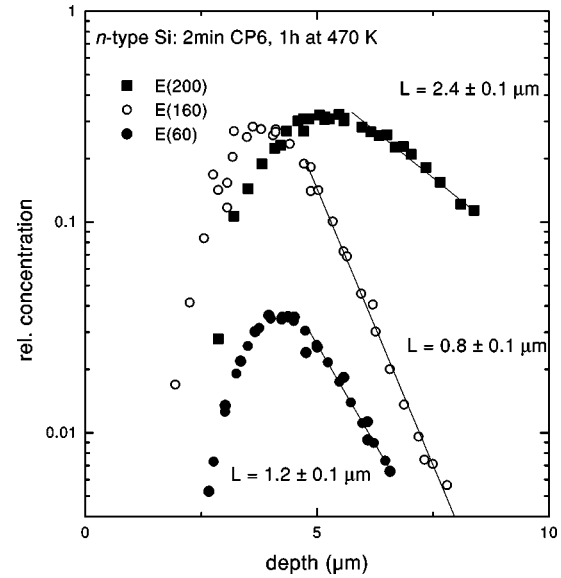


FIG. 7. Depth profiles of PdH defects in *n*-type Si after wet-chemical etching and annealing at 470 K for 1 h.

nealed above 450 K. Under these conditions, we find a total dissociation of all boron and phosphorus-hydrogen pairs. Annealing above 450 K leads to the decrease of all new hydrogen levels and the formation of another complex, which is only indirectly accessible in *n*- and *p*-type samples.

Figure 7 gives the profiles of the hydrogen-induced levels in Pd-doped *n*-type samples. The concentrations are given relative to the substitutional Pd concentration detected in cleaved samples. After wet-chemical etching, the sample was annealed at 470 K for 1 h. The profiles of the three PdH levels show pronounced exponential decrease for larger depth. All three PdH levels exhibit a different slope. The characteristic length of the decay is  $3.6 \pm 1 \mu\text{m}$  for  $E(200)$ ,  $1.2 \pm 1 \mu\text{m}$  for  $E(160)$ , and  $1.8 \pm 1 \mu\text{m}$  for  $E(60)$ . The defect profiles show the expected integer ratios for the characteristic length. We assume that  $E(200)$  belongs to the  $\text{PdH}_1$  complex, which has the largest penetration into the sample. The ratio  $L_{E(200)}/L_{E(60)}=2$  relates  $E(60)$  to a  $\text{PdH}_2$  complex,  $L_{E(200)}/L_{E(160)}=3$  associates  $E(160)$  with a  $\text{PdH}_3$  complex.

In the *n*-type sample the concentration of the  $\text{PdH}_3$  complex is much higher than the concentration of the  $\text{PdH}_2$  complex. This is in contrast to the Pt case, where for larger depth the  $\text{PtH}_1$  complex was always strongest, followed by the  $\text{PtH}_2$  and  $\text{PtH}_3$  complex. The behavior in Pd-doped samples indicates a complication in the simple model presented above for the formation of the complexes. A possible explanation will be given below.

### 2. *p*-type samples

A profile from a *p*-type sample after wet-chemical etching and annealing for 1 h at 470 K is shown in Fig. 8. Again, the concentrations are given relative to the total substitutional Pd concentration determined before wet-chemical etching. The semilogarithmic plot gives an exponential decrease of the defect concentrations with depth. The profiles of the four levels can be grouped into two sets with similar slopes at

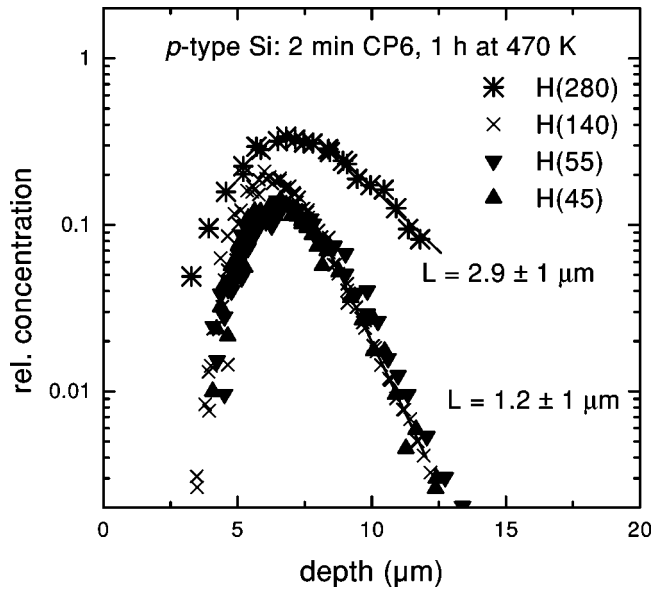


FIG. 8. Depth profiles of PdH defects in *p*-type Si after wet-chemical etching and annealing at 470 K for 1 h.

larger depth. Level H(280) is characterized by a slope with the largest characteristic length of  $L = 2.9 \pm 1 \mu\text{m}$ . The profiles for H(45), H(55), and H(140) are not distinguishable at larger depth and show the same slope of  $L = 1.2 \pm 1 \mu\text{m}$ . Usually, this behavior is evidence for hydrogen complexes that involve the same number of hydrogen atoms. Contrary to the *n*-type sample, the ratio of the two slopes gives no clear identification of the number of hydrogen atoms involved in the complexes.

The levels H(45), H(55), and H(140) exhibit the same slope for larger depth, but H(140) has a higher maximum concentration. The difference in concentration can be related to another PdH level, which overlaps strongly with H(140) and is only visible in the range from 5 to 7  $\mu\text{m}$ . If we subtract the profile of H(55) from H(140), we receive a profile with a steep slope of  $L = 0.6 \pm 0.2 \mu\text{m}$ , indicating an incorporation of around 5–7 hydrogen atoms in the complex.

### 3. Comparison of profiles in *n*- and *p*-type Si

In the Pd-doped samples a direct comparison of the depth profiles in *n*- and *p*-type samples is possible and allows a correlation of defect levels belonging to the same center. As discussed already above, only profiles of samples that were annealed above 450 K were considered to avoid complications from acceptor or donor hydrogen formation. The influence of different Pd doping levels in the samples is corrected by scaling the profile of the Pd acceptor in *n*-type Si to the Pd donor level in *p*-type Si. Figure 9 gives the result of the scaling process. The profiles of the Pd donor, double donor, and acceptor are now identical. The profiles of the PdH defects are scaled with the same factor. The result is given in Fig. 10. For clarity only the profiles for the levels *E*(200), H(280), *E*(160), H(55), and *E*(60) are given. The missing profile H(45) is identical to H(55), and the properties of H(140) were discussed already. The error bar in concentration and depth is estimated to be 10% of the values given in the figure.

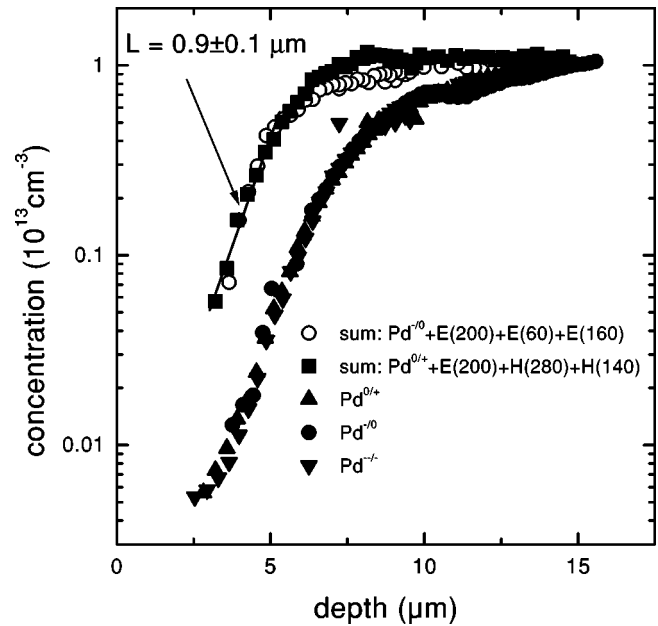


FIG. 9. Profiles of the three substitutional Pd levels:  $\text{Pd}^{-/0}$ ,  $\text{Pd}^{0/+}$ ,  $\text{Pd}^{+/-}$  after scaling (for details see text). The sum of all electrically active Pd defect levels is included.

The levels can be grouped again according to their slopes at larger depth. From the ratios of the characteristic length, an identification of the number of hydrogen atoms involved in the complexes can be made. In the *n*-type sample *E*(200) was already assigned to the  $\text{PdH}_1$  complex, *E*(60) to the  $\text{PdH}_2$  complex, and *E*(160) to the  $\text{PdH}_3$  complex. The profile of H(45), H(55), and H(140) coincides with that of *E*(160) for larger depth, indicating that all these levels belong to a  $\text{PdH}_3$  complex. However, there is a problem with the assignment of *E*(160), H(55), and H(45) to the  $\text{PdH}_3$  complex. One would expect that all profiles coincide everywhere in the whole sample. But level *E*(160) has a higher maximum concentration compared to the H(55) and H(45)

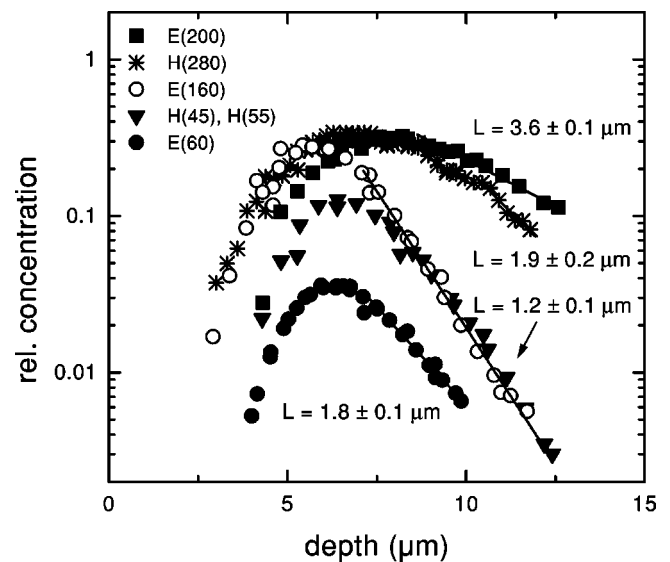


FIG. 10. Depth profiles of all PdH defects in *p*- and *n*-type Si after wet-chemical etching and annealing at 470 K for 1 h.

levels. This could be explained again by a level of an additional PdH complex that is overlapping with the  $E(160)$  DLTS peak. However, the difference of the profiles  $E(160)$  and  $H(55)$  gives a slope that is very steep, corresponding to Pd complexes of at least ten hydrogen atoms. It is not realistic that these complexes are formed in such high concentrations.

Level  $H(280)$  has a very similar profile as  $E(200)$ , the  $\text{PdH}_1$  complex; the concentration of  $H(280)$  is lower at larger depth and larger closer to the surface where hydrogen concentration increases. This behavior indicates that  $H(280)$  belongs to a complex with more than one hydrogen atom but less than three hydrogen atoms. Tentatively, we have fitted in Fig. 10 the last part of the profile to get a slope corresponding to a  $\text{PdH}_2$  complex. With the assignment of  $H(280)$  to the  $\text{PdH}_2$  complex an obvious difficulty occurs: the concentration of the  $\text{PdH}_2$  complex in  $p$ - and  $n$ -type samples is quite different, as is evidenced from the profiles of  $H(280)$  and  $E(60)$ .

We can resolve the difficulties by reevaluating the approximations made in modeling the formation process of the hydrogen defects. A major simplification in the differential equations [Eq. (3)], which describe the depth profiles of the hydrogen complexes, is the use of charge-state independent capture radii  $r_i$ . In the  $n$ -type samples obviously a much faster trapping of hydrogen to the  $\text{PdH}_2$  complex seems to occur, compared to  $p$ -type samples. This leads to a strongly reduced  $\text{PdH}_2$  and an increased  $\text{PdH}_3$  concentration in  $n$ -type samples. The behavior is different in Pt-doped samples and can be related to the level position of the  $\text{PdH}_2$  complex. In  $n$ -type samples at the temperature of annealing, most of the  $\text{PdH}_2$  complexes are in the negative state, and an efficient trapping by positively charged hydrogen occurs. In  $p$ -type samples the  $\text{PdH}_2$  complex is neutral and trapping by the positively charged hydrogen is less efficient. The  $H(210)$  level of the  $\text{PdH}_2$  is closer to the valence band, which leads in  $n$ - and  $p$ -type samples to the same interaction of the negatively charged  $\text{PtH}_2$  complex with positively charged hydrogen.

The behavior of the  $\text{PdH}_2$  depth profile in  $p$ -type samples needs further discussion. As we have discussed above, the proper slope can only be found for very large depth. The total concentration of the  $\text{PdH}_2$  complex is identical to that of the  $\text{PdH}_1$  complex at the maximum. Apparently for the PdH complexes the capture radii are not decreasing with complex size, as was found for Pt-doped samples. To explain the behavior of the  $\text{PdH}_2$  depth profile in  $p$ -type samples, we have to assume a much faster capture of H to  $\text{PdH}_1$  than H to Pd. In the extreme case—no more hydrogen capture to Pd—the  $\text{PdH}_2$  concentration would follow the  $\text{PdH}_1$  profile. Only for small hydrogen concentrations, which occur at larger depth, the  $\text{PdH}_2$  profile will follow the expected slope.

Our interpretation of the PdH profiles is in close analogy to the case in Pt-doped samples, but refinements in the simple model of the successive capture of hydrogen atoms to the defects have to be included. First, a different capture rate for  $n$ - and  $p$ -type samples is necessary to account for the  $\text{PdH}_2$  profiles. Second, the capture radii of higher complexes can be larger than those of lower complexes ( $r_i \leq r_{i+1}$ ).

### C. Identification of a passive PdH complex

In Fig. 9 we have included the profile of the total concentration of all Pd complexes. Two different summations are used. The first sum adds up over levels in the upper half of the band gap,

$$\sum = \text{Pd}^{-/0} + E(200) + E(60) + E(160). \quad (5)$$

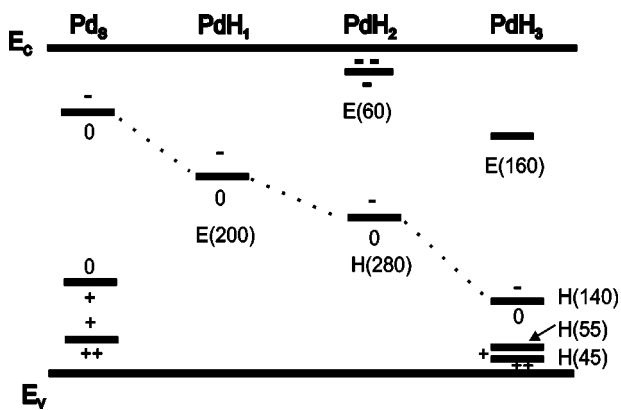
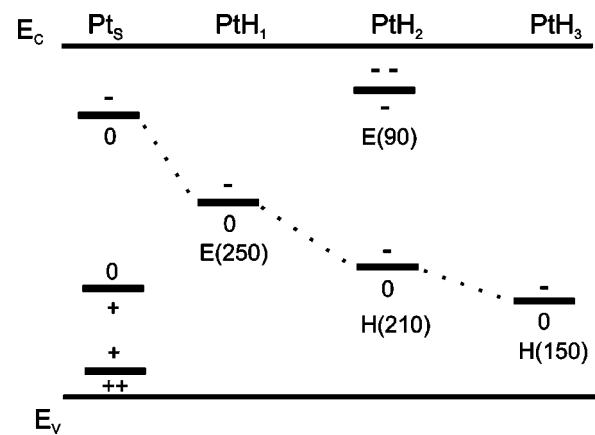
The second sum uses for substitutional Pd and the  $\text{PdH}_2$  and  $\text{PdH}_3$  complexes the levels from the lower half of the band gap,

$$\sum = \text{Pd}^{0/+} + H(280) + H(140). \quad (6)$$

Both summations give within the error the same results. In the range from 4 to 6  $\mu\text{m}$ , the concentration of the sum is identical to the substitutional concentration in the cleaved sample. This behavior indicates that all Pd-correlated complexes are properly included in the summation. Below 4  $\mu\text{m}$  the total concentration of Pd-related centers decreases strongly towards the surface. Because all electrically active defects are included in this profile, the decrease has to be due to the formation of an electrically passive PdH defect, which is only formed in the region with the highest hydrogen concentration. We therefore assume that the passive complex contains at least four hydrogen atoms. Close to the surface this complex leads to a total passivation of Pd, and after annealing at 470 K this passive complex dominates all other electrically active hydrogen complexes. Above 550 K the passive complex dissociates into substitutional Pd and hydrogen. At present, we cannot distinguish between one or several different passive complexes. If we assume, however, that only one passive PdH complex exists, we can analyze the slope of the sum curve. The characteristic length for the passive complex is given by  $L = 0.9 \pm 1 \mu\text{m}$ . This would make the passive complex a  $\text{PdH}_4$  complex.

### D. Comparison with previous DLTS studies on Pd-doped silicon

Several studies in Pd-doped Si revealed levels that are very similar to our hydrogen-related centers. In all these studies wet-chemical etching was applied before the contact preparation, which could unintentionally introduce hydrogen into the samples. Lemke observed in  $p$ -type Si after annealing a level at  $E_V + 0.26 \text{ eV}$ .<sup>30</sup> The properties of this level seem to be identical with our  $H(140)$  level. Stöffler and Weber<sup>39</sup> and Czupata *et al.*<sup>34,40</sup> detected in diffused  $n$ -type samples two levels with activation energies very similar to  $E(160)$  and  $E(200)$ . Depth profiles from Pd-doped samples reported by Gill *et al.* give a level at  $E_C - 0.37 \text{ eV}$  with a strong decrease in concentration towards the bulk.<sup>41</sup> In comparison with the results from our study, a correlation with the two levels  $E(160)$  and  $E(200)$  is possible. However, the level observed by Gill *et al.* anneals out already at  $150^\circ\text{C}$ , whereas  $E(160)$  and  $E(200)$  are much more stable. In addition, the authors of Ref. 41 associate this level with another level at  $E_C - 0.59 \text{ eV}$ , which was never detected in our

FIG. 11. Energy levels of substitutional Pd and PdH<sub>i</sub> complexes.FIG. 12. Energy levels of substitutional Pt and PtH<sub>i</sub> complexes.

samples. The only report of an interaction of hydrogen with Pd was given by Pearton and Haller.<sup>21</sup> A plasma treatment at 300 °C for 2 h led to a total passivation of the substitutional Pd donor and acceptor state. No other levels were generated under these conditions. This result is in agreement with our measurements. At 300 °C the passive complex still dominates at the surface, and all other hydrogen-related complexes are very weak.

### E. Comparison of PdH and PtH levels

Figure 11 gives schematically the derived level positions for the different PdH<sub>i</sub> complexes. A clear trend for the acceptor level is seen, which systematically is lowered with the addition of another hydrogen to the defect. This behavior can be expected from the simple vacancy model of the substitutional TM's. The  $t_2$  level of the vacancy shifts towards the valence band for increasing nuclear charge. Apparently, the addition of protons has the same effect as increasing the nuclear charge.

The behavior of PtH complexes in Si was studied by several groups. From the analysis of the deep-level profiles, three electrically active PtH complexes were determined, which contained one, two, or three hydrogen atoms.<sup>20</sup> The PtH<sub>4</sub> complex was associated with an electrically neutral complex. A correlation was made for the levels of the PtH<sub>2</sub> complex with IR absorption lines and an EPR spectrum.<sup>16–18</sup>

Figure 12 gives a level scheme of the PtH<sub>i</sub> complexes for comparison. We find qualitatively the same trends in the Pt and Pd samples; however, the number of hydrogen-induced levels is larger in the Pd case. For the PtH<sub>i</sub> levels the charge states were determined by studying the behavior of the levels in an electrical field and by temperature-dependent CV measurements.<sup>19,20</sup> For Pd complexes the charge states for levels E(60), H(45), and Pd<sup>+/++</sup> were identified from the electrical-field dependence of the level energies and the temperature dependence of the capture cross section. All the other levels did not show any field dependence. In Fig. 11 we assigned the charge states for these levels in analogy to the Pt case.

### F. Result of theoretical calculations on the PdH levels

Recently, numerical techniques were developed that allow a precise determination of the TM levels in Si and their hy-

drogen complexes.<sup>42</sup> The level positions were calculated compared to a reference level of a well-defined defect. The calculations by Jones *et al.*<sup>43</sup> give for the PdH<sub>1</sub> complex an acceptor level at  $E_C - 0.30$  eV in close agreement with E(200) at  $E_C - 0.43$  eV. The acceptor level shifts weakly in the PdH<sub>2</sub> complex to  $E_C - 0.36$  eV, which corresponds to H(280) at  $E_V + 0.55$  eV. The error in calculating the acceptor level of the PdH<sub>3</sub> complex is estimated to be much larger due to the method of calculation. The acceptor level was calculated at  $E_C - 1.15$  eV compared to  $E_C - 0.93$  eV for the H(140) level. Further agreement can be found for the double acceptor state of the PdH<sub>3</sub> complex: The calculated value of  $E_C - 0.29$  eV could correspond to  $E_C - 0.29$  eV of the E(160) level. From our experiments no assignment to a double acceptor state could be made.

There are, however, also some discrepancies between the theoretical results and our assignment of the levels. Jones *et al.* calculate a donor level for the PdH<sub>1</sub> complex at  $E_V + 0.62$  eV. This level does not appear in our experiments. The proposed coincidence of this level with the level of the Pd donor Pd<sup>0/+</sup> can be excluded from the identical profiles for the Pd donor and double donor (Pd<sup>0/+</sup>, Pd<sup>+/++</sup>). The calculations give for the PdH<sub>4</sub> complex an acceptor and a donor level. No support is given from the calculation that a substitutional PdH defect is electrically passive. This strongly contradicts the measurements where an electrically inactive complex accounts for the missing concentration of all electrically active Pd defects in the sample. The suggestion of a formation of neutral PdH species in cavities or microvoids is not realistic. Wet-chemical etching and additional annealing steps are not suited to form these microdefects. Also, the reactivation of the substitutional Pd at higher temperatures leads to a distribution of substitutional Pd, as was found originally in the cleaved sample. A passive PdH<sub>4</sub> complex that involves the substitutional Pd would be the simplest explanation of our results.

We have found from the difference in the profiles for the H(140) and the H(55) levels evidence for another PdH species with a depth profile that would associate this level with a PdH complex that contains at least five to seven hydrogen atoms. Further studies with higher original hydrogen concentrations should clarify the existence of electrical PdH levels with more than four hydrogen atoms.

## V. CONCLUSIONS

We have studied the interaction of hydrogen with substitutional Pd in Si. A careful investigation of the electrical properties of wet-chemically etched samples revealed seven different hydrogen-induced levels. From analysis of the defect profiles, we were able to correlate these levels to Pd complexes that contain up to three hydrogen atoms. A neutral Pd hydrogen complex is found to contain four hydrogen atoms. Evidence of at least one electrically active complex with more than four hydrogen atoms is presented. The behavior of the PdH complexes is very similar to PtH complexes; however, some refinements in the simple model of hydrogen defect formation have to be included for the Pd complexes. The trend of the energy levels with the number

of hydrogen atoms in the complexes reflects the simple vacancylike structure of the complexes.

## ACKNOWLEDGMENTS

We thank M. Stavola and R. Jones for many helpful discussions and comments. H. J. Queisser gave steady support throughout this work. G. I. Andersson (Chalmers University of Technology, Göteborg, Sweden) provided the original computer program for depth profile calculations. We acknowledge the technical assistance and continuous help of W. Heinz and W. Krause. A. Mesli gave valuable advice and help with the MCT measurements. We acknowledge support from W. Schröter and H. Riemann from the Institut für Kristallzüchtung (Berlin), where the float-zone Si samples were grown.

- <sup>1</sup>H. H. Woodbury and G. W. Ludwig, Phys. Rev. **126**, 466 (1962).
- <sup>2</sup>K. Graff, *Metal Impurities in Silicon Device Production* (Springer-Verlag, Berlin, 1995).
- <sup>3</sup>G. D. Watkins, Physica B & C **117B&118B**, 9 (1983).
- <sup>4</sup>H. Zimmermann and H. Ryssel, Appl. Phys. Lett. **58**, 499 (1991).
- <sup>5</sup>J.-U. Sachse, W. Jost, J. Weber, and H. Lemke, Appl. Phys. Lett. **71**, 1379 (1997).
- <sup>6</sup>E. Ö. Sveinbjörnsson and O. Engström, Appl. Phys. Lett. **61**, 2323 (1992).
- <sup>7</sup>E. Ö. Sveinbjörnsson and O. Engström, Phys. Rev. B **52**, 4884 (1995).
- <sup>8</sup>T. Sadoh, H. Nakashima, and T. Tsurushima, J. Appl. Phys. **72**, 520 (1992).
- <sup>9</sup>T. Sadoh, M. Watanabe, H. Nakashima, and T. Tsurushima, J. Appl. Phys. **75**, 3978 (1994).
- <sup>10</sup>W. Jost, J. Weber, and H. Lemke, Semicond. Sci. Technol. **11**, 22 (1996).
- <sup>11</sup>W. Jost, J. Weber, and H. Lemke, Semicond. Sci. Technol. **11**, 525 (1996).
- <sup>12</sup>W. Jost and J. Weber, Phys. Rev. B **54**, R11 038 (1996).
- <sup>13</sup>J.-U. Sachse, E. Ö. Sveinbjörnsson, W. Jost, J. Weber, and H. Lemke, Appl. Phys. Lett. **70**, 1584 (1997).
- <sup>14</sup>J.-U. Sachse, E. Ö. Sveinbjörnsson, N. Yarykin, and J. Weber, Mater. Sci. Eng., B **58**, 134 (1999).
- <sup>15</sup>N. Yarykin, J.-U. Sachse, H. Lemke, and J. Weber, Phys. Rev. B **59**, 5551 (1999).
- <sup>16</sup>P. M. Williams, G. D. Watkins, S. Uftring, and M. Stavola, Phys. Rev. Lett. **70**, 3816 (1993).
- <sup>17</sup>M. Höhne, U. Juda, Y. V. Martynov, T. Gregorkiewicz, C. A. J. Ammerlaan, and L. S. Vlasenko, Phys. Rev. B **49**, 13 423 (1994).
- <sup>18</sup>S. J. Uftring, M. Stavola, P. M. Williams, and G. D. Watkins, Phys. Rev. B **51**, 9612 (1995).
- <sup>19</sup>J.-U. Sachse, E. Ö. Sveinbjörnsson, W. Jost, J. Weber, and H. Lemke, Phys. Rev. B **55**, 16 176 (1997).
- <sup>20</sup>J.-U. Sachse, J. Weber, and E. Ö. Sveinbjörnsson, Phys. Rev. B **60**, 1474 (1999).
- <sup>21</sup>S. J. Pearton and E. E. Haller, J. Appl. Phys. **54**, 3613 (1983).
- <sup>22</sup>J.-U. Sachse, J. Weber, and H. Lemke, Mater. Sci. Forum **258-263**, 307 (1997).
- <sup>23</sup>H. Lemke, in *Semiconductor Silicon*, edited by H. R. Huff, W. Bergholz, and K. Sumino (Electrochemical Society, Pennington, NJ, 1994), p. 695.
- <sup>24</sup>H. G. Grimmeiss, E. Janzén, B. Skarstam, and A. Lodding, J. Appl. Phys. **51**, 6238 (1980).
- <sup>25</sup>D. V. Lang, J. Appl. Phys. **45**, 3023 (1974).
- <sup>26</sup>B. Hamilton, A. R. Peaker, and D. R. Wight, J. Appl. Phys. **50**, 6373 (1979).
- <sup>27</sup>J. A. Davidson and J. H. Evans, Semicond. Sci. Technol. **11**, 1704 (1996).
- <sup>28</sup>J. A. Pals, Solid-State Electron. **17**, 1139 (1974).
- <sup>29</sup>J. W. Chen and A. G. Milnes, Annu. Rev. Mater. Sci. **10**, 157 (1980), and references therein.
- <sup>30</sup>H. Lemke, Phys. Status Solidi A **86**, K39 (1984).
- <sup>31</sup>A. Mirzaev, Sh. Makhamov, and N. A. Tursunov, Fiz. Tekh. Poluprovodn. **22**, 1177 (1988) [Sov. Phys. Semicond. **22**, 746 (1988)].
- <sup>32</sup>J. Vicente, J. L. Enríquez, E. Rubio, L. Bailón, and J. Barbolla, J. Electrochem. Soc. **140**, 868 (1993).
- <sup>33</sup>T. Zundel and J. Weber, Phys. Rev. B **39**, 13 549 (1989).
- <sup>34</sup>R. Czupata, M. Midl, H. Feichtinger, and A. Bauer, Mater. Sci. Forum **38-41**, 415 (1989).
- <sup>35</sup>Zhou Jie, R. Shengyang, H. Hong, G. Weikun, J. Xiujiang, and L. Shuying, Mater. Sci. Forum **10-12**, 723 (1986).
- <sup>36</sup>J. Zhu, N. M. Johnson, and C. Herring, Phys. Rev. B **41**, 12 354 (1990).
- <sup>37</sup>A. L. Endrös, W. Krühler, and J. Grabmaier, Physica B **170**, 365 (1991).
- <sup>38</sup>O. V. Feklisova and N. A. Yarykin, Semicond. Sci. Technol. **12**, 742 (1997).
- <sup>39</sup>W. Stöffler and J. Weber, Mater. Sci. Forum **10-12**, 705 (1986).
- <sup>40</sup>R. Czupata, Appl. Phys. A: Solids Surf. **49**, 431 (1989).
- <sup>41</sup>A. A. Gill, M. Z. Iqbal, and N. Zafar, Semicond. Sci. Technol. **8**, 675 (1993).
- <sup>42</sup>A. Resende, R. Jones, S. Öberg, and P. R. Briddon, Phys. Rev. B **82**, 2111 (1999).
- <sup>43</sup>R. Jones, A. Resende, S. Öberg, and P. R. Briddon, Mater. Sci. Eng., B **58**, 113 (1999).